

Conformal diffusion acoustic metasurfaces with soft materials for scattering reduction

Kunhong Li(李昆鸿), Wenkang Cao(曹文康), Qiao Huang(黄桥), Jinsong Ye(叶劲松), Kaiping Nie(聂开萍), and Jie Hu(胡捷)

Citation: Chin. Phys. B, 2026, 35 (**6**): 064301. DOI: 10.1088/1674-1056/ae2bf0
http://cpb.iphy.ac.cn; http://iopscience.iop.org/cpb

What follows is a list of articles you may be interested in

Generalized likelihood ratio detector for forward scattering detection in uncertain shallow-water environments

Jiahui Luo(罗嘉辉), Chao Sun(孙超), Mingyang Li(李明杨), and Shaodong Zhang(张少东)
Chin. Phys. B, 2026, 35 (**5**): 054303. DOI: 10.1088/1674-1056/ae118f

Energy focusing of flexural waves via algorithmically optimized coding metasurface lenses

Zi-Rui Wang(王子睿), Di-Chao Chen(陈帝超), Rui Hong(洪瑞), and Da-Jian Wu(吴大建)
Chin. Phys. B, 2025, 34 (**9**): 094302. DOI: 10.1088/1674-1056/add1be

High-order Bragg forward scattering and frequency shift of low-frequency underwater acoustic field by moving rough sea surface

Ya-Xiao Mo(莫亚枭), Chao-Jin Zhang(张朝金), Li-Cheng Lu(鹿力成), Qi-Hang Sun(孙启航), and Li Ma(马力)
Chin. Phys. B, 2024, 33 (**3**): 034301. DOI: 10.1088/1674-1056/ad108f

One-dimensional PT-symmetric acoustic heterostructure

Hai-Xiao Zhang(张海啸), Wei Xiong(熊威), Ying Cheng(程营), and Xiao-Jun Liu(刘晓峻)
Chin. Phys. B, 2022, 31 (**12**): 124301. DOI: 10.1088/1674-1056/ac90b3

Simulation of detection and scattering of sound waves by the lateral line of a fish

V M Adamyan, I Y Popov, I V Blinova, and V V Zavalniuk
Chin. Phys. B, 2022, 31 (**2**): 024301. DOI: 10.1088/1674-1056/ac1b81

Conformal diffusion acoustic metasurfaces with soft materials for scattering reduction

Kunhong Li(李昆鸿), Wenkang Cao(曹文康)[†], Qiao Huang(黄桥), Jinsong Ye(叶劲松), Kaiping Nie(聂开萍), and Jie Hu(胡捷)[‡]

School of Mechanical Engineering, Guizhou University, Guiyang 550025, *China*

(Received 24 September 2025; revised manuscript received 9 December 2025; accepted manuscript online 12 December 2025)

Planar diffusion acoustic metasurfaces (PDAMs) with rigid materials have attracted much attention due to their ability to redistribute acoustic energy in various directions and to realize acoustic stealth. In this paper, to enhance the adaptability of PDAMs to complex curved surfaces, a conformal diffusion acoustic metasurface (CDAM) with soft materials is proposed to manipulate scattering features, leading to considerable scattering reduction in the specular direction. To realize the proposed CDAM, eight kinds of meta-atoms with phase differences of 45° are introduced. Polydimethylsiloxane (PDMS) is chosen as the material of meta-atoms, which not only has a low modulus but also possesses the ability to deform compliantly with environmental conditions. The simulated results demonstrate that the proposed CDAM can achieve backward scattering reduction of at least 9 dB with bending angles of the CDAM from 0° to 90°, and has potential applications in noise control, acoustic stealth, architectural acoustics, and other relevant applications.

Keywords: conformal diffusion acoustic metasurface, scattering reduction, soft materials, coding metasurface

PACS: 43.20.Fn, 43.20.+g, 43.35.+d

DOI: 10.1088/1674-1056/ae2bf0 **CSTR:** 32038.14.CPB.ae2bf0

1. Introduction

Over the past few decades, acoustic metamaterials have garnered significant attention due to their unique ability to manipulate acoustic waves. As two-dimensional (2D) forms, acoustic metasurfaces have gained favor among researchers due to their efficient wavefront manipulation capabilities, compact thickness, and low material loss compared to traditional acoustic metamaterials.[1–4] These metasurfaces achieve extraordinary control over sound by locally regulating the amplitude and phase responses of meta-atoms at subwavelength scales and assembling them into structural arrays.[5–8] These characteristics enable broad application prospects in multiple fields, such as asymmetric transmission,[9,10] acoustic holography,[11,12] acoustic absorption,[13,14] and beam splitting.[15]

Recently, acoustic metasurfaces have been employed to manipulate scattering features and obtain sound-diffusion reflection, achieving the phenomenon of acoustic stealth. As early as the 1970s, Schroeder[16,17] proposed the concept of the acoustic diffuser, which can be used to uniformly scatter sound in different directions, and these studies opened a new field. However, these traditional acoustic diffusers have faced significant drawbacks in practical engineering applications due to several issues, such as bulky structures and irregular surfaces. Therefore, acoustic diffusers based on metasurfaces with compact structures and regular surfaces have emerged.[18,19] To be specific, an ultrathin Schroeder diffuser with a thickness of $\lambda/20$ (λ is the wavelength of acoustic waves) has been proposed based on acoustic metasurfaces.[20] In order to overcome the fundamental limitations of Schroeder diffusers in intensity uniformity and narrow bandwidth, a mechanism using a smooth distribution of the reflected phase on the surface of the acoustic diffuser was proposed.[21] Subsequently, a spiral acoustic metasurface based on holographic acoustic vortices has been proposed, capable of achieving wideband and high uniformity in sound diffusion, thereby effectively suppressing specular reflection.[22] In addition, a lightweight membrane-type resonator-based Schroeder diffuser, which consists of a decorated membrane and a rigid back cavity, was demonstrated to produce a high-efficiency diffuse sound field.[23] A broadband acoustic metaveil composed of a configurable array of two acoustic meta-atoms was proposed, which can achieve undistorted transmission and diffuse reflection simultaneously.[24] In addition, for underwater scenes, an ultrathin reflective pentamode metasurface at frequencies below 1000 Hz was proposed to realize uniform diffuse reflections.[25] As aforementioned, the incoming energy of acoustic waves can be redistributed in selected directions, and excellent backward scattering reduction can be achieved via these acoustic diffusion metasurfaces.

Additionally, as an efficient and flexible strategy for wavefront manipulation, coding sequences enable precise manipulation of acoustic responses,[26,27] such as the phase and amplitude of acoustic waves, through coding logic, thereby

[†]Corresponding author. E-mail: wkcao@gzu.edu.cn

[‡]Corresponding author. E-mail: jiehu@gzu.edu.cn

© 2026 Chinese Physical Society and IOP Publishing Ltd. All rights, including for text and data mining, AI training, and similar technologies, are reserved.

providing a straightforward pathway for realizing complex acoustic functionalities. This concept is realized by acoustic coding metasurfaces composed of meta-atoms arranged according to pre-designed coding sequences, which have emerged recently, offering a new route to enhancing the flexibility of wavefront manipulation and improving the performance of diffusers.[28,29] Only a finite number of meta-atoms are required to control the energy distribution of reflected waves, which greatly simplifies the design and optimization of the scattering pattern of acoustic diffusers. To be specific, a reflection-type acoustic metasurface diffuser based on coding metasurfaces was designed by arranging two types of unit cells with opposite phase responses in a specific sequence, dispersing the incident acoustic energy in multiple directions, effectively suppressing specular reflection and achieving sound diffusion.[30] Similarly, an underwater acoustic coding metasurface based on pentamode metamaterials, composed of two types of hexagonal unit cells, was proposed. By arranging them into an array according to a random 1-bit coding sequence, a low-scattering underwater acoustic stealth effect over a wide range of incident angles is obtained.[31] In addition, in order to enhance scattering reduction performance, an acoustic coding metasurface integrating diffusion and absorption has also been proposed. This absorption–diffusion integrated mechanism can further disperse incoming energy and improve acoustic stealth performance.[32] The above acoustic diffusers based on coding metasurfaces are encoded and spatially arranged through random or optimized coding sequences, introducing carefully engineered phase transitions during reflection. Leveraging coherent diffraction effects, the incident acoustic energy is dispersed in multiple directions, ultimately achieving highly efficient acoustic diffusion.

However, although existing acoustic meta-diffusers have achieved scattering reduction, these investigations are limited to planar structures with rigid materials. Hence, structural deformability and adaptability to external environments remain insufficient. Thus, nonplanar or curved acoustic metasurfaces offer a new avenue of research and have attracted considerable interest. Specifically, a reconfigurable curved acoustic metasurface was reported for acoustic cloaking and illusion, which is composed of an array of tunable helical units.[33] An acoustic antenna with arbitrarily curved configurations was proposed to realize beamforming in arbitrary directions.[34] A conformal acoustic metasurface was presented, which utilizes conformal ultrathin coatings to reshape the reflected wavefront of an object.[35] In addition, curved acoustic adaptive metasurfaces for underwater applications have also been reported, which are composed of four absorptive elements and maintain excellent low-frequency broadband sound absorption performance.[36] A curved conformal acoustic metasurface coating with fan-shaped ultrathin labyrinth channels for underwater pipeline noise control has been proposed.[37] In addition, recent studies have explored soft acoustic metasurfaces for sound control, which are based on soft materials referring not only to low-modulus mechanical properties but also to the ability to deform compliantly with external environments. For example, a soft acoustic metasurface constructed by embedding bubbles within soft materials enables full-phase modulation of underwater acoustic waves through adjustment of bubble size, facilitating acoustic stealth and beam manipulation.[38] An acoustic metasurface based on soft gradient refractive-index porous silicone rubber enables efficient broadband ultrasonic wavefront manipulation, including acoustic beam deflection, focusing, and vortex generation.[39] An ultrathin acoustic metasurface composed of a porous network of soft polymer fibers and rigid beads has been fabricated, enabling efficient wavefront manipulation, including acoustic vortices, focusing, and super-oscillation.[40] An acoustic metasurface based on soft porous polymers has been demonstrated to achieve efficient manipulation of underwater ultrasonic wavefronts through precise control of material porosity.[41] Nevertheless, although these acoustic metasurfaces have achieved significant progress, diffusion acoustic metasurfaces with nonplanar structures and soft materials remain insufficiently explored, despite their ability to conform to complex curved surfaces and significantly enhance practical utility.

In this paper, a conformal diffusion acoustic metasurface (CDAM) using soft materials is proposed, which can achieve considerable scattering reduction in specular directions at different bending angles. To achieve this, cavity-structured meta-atoms are designed and polydimethylsiloxane (PDMS) is chosen as the material. Geometric parameter tuning enables a reflection phase coverage of more than 315° while maintaining subwavelength thickness. The resulting meta-atoms are arranged in a quasi-random coding sequence to construct a 3-bit coding metasurface for scattering reduction, and the soft material enables conformal adaptation to curved surfaces. Numerical simulations confirm efficient sound diffusion for both planar and curved configurations, achieving more than 9 dB scattering reduction compared with shape-matched rigid plates. Unlike traditional acoustic diffusers, the CDAM enables robust sound diffusion and reflection suppression across multiple curved geometries, making it suitable for stealth applications and noise control on complex surfaces.

2. Design principle of the CDAM and meta-atoms

Figure 1 shows the schematic diagram of the CDAM proposed in this paper. The CDAM is composed of eight kinds of coding elements (meta-atoms), labeled 0 to 7 and represented by different colors. The phase difference between adjacent

meta-atoms is approximately 45°. By controlling the structural parameters of the meta-atoms, a reflection phase coverage of more than 315° can be obtained, as will be demonstrated later, thereby achieving the required phase response. Moreover, the coding elements are arranged in a quasi-random fashion. Under plane-wave illumination at an operating frequency of 3430 Hz, the energy of incident waves is dispersed in all directions due to destructive interference between coding elements. In addition, since PDMS is used as the material for the proposed CDAM, it can be deformed to adapt to different curved surfaces, significantly enhancing the applicability of diffusion acoustic metasurfaces.

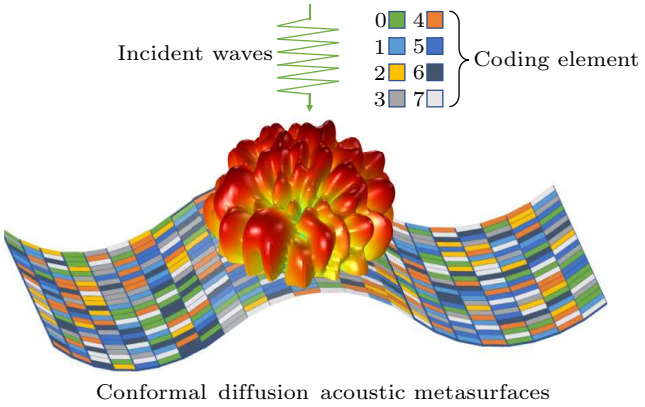


Fig. 1. Schematic diagram of the proposed CDAM, composed of eight types of coding elements represented by different colors. Under plane-wave illumination, the incident acoustic energy is dispersed in all directions.

To achieve the required meta-atoms with phase differences of 45°, Figs. 2(a) and 2(b) show the three-dimensional (3D) schematic diagram and cross-sectional view of the proposed meta-atom, which is a Helmholtz-resonance-like structure. The meta-atom is made of PDMS, a soft material with a mass density of 970 kg/m^3, sound velocity of 1028 m/s, Young's modulus of 750 kPa, and Poisson's ratio of 0.49. Furthermore, the acoustic loss of PDMS is shown to be negligible around the target operating frequency, as detailed in the supplementary material. The background medium is air with a mass density of 1.29 kg/m^3 and sound velocity of 343 m/s. Here, the meta-atom consists of double cuboid cavities with widths w and w_1, respectively. The total height, wall thickness, and period of the meta-atom are denoted as h, t, and a. The specific parameters are fixed at $a = 25$ mm, $h = 5$ mm, $t = 1$ mm, $w_1 = 23$ mm, and the width of the upper cuboid cavity w can be adjusted to achieve the required phase coverage of reflected waves. To demonstrate the performance of the proposed meta-atoms, simulations are performed using the pressure acoustics, solid mechanics, and thermoviscous acoustics modules in the commercial software COMSOL Multiphysics 6.2. Periodic boundary conditions are applied around the unit cell, and a plane wave is incident along the $-z$ direction with different incidence angles, defined as the angle between the incident direction and the surface normal.

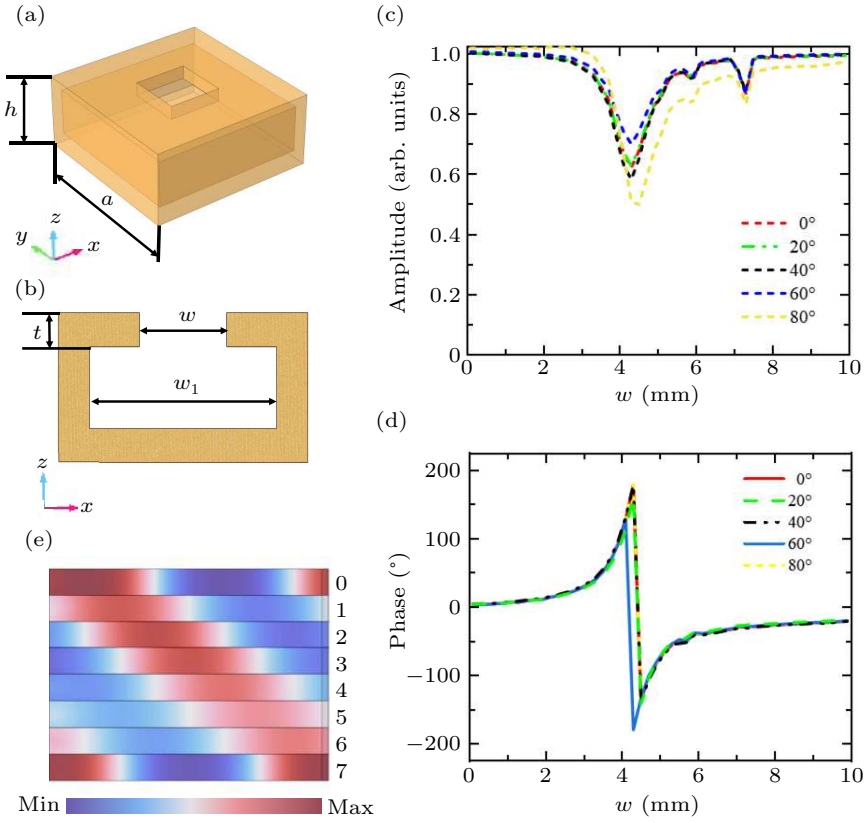


Fig. 2. (a), (b) Schematic of the proposed CDAM meta-atom and its corresponding cross-sectional view. (c), (d) Reflection amplitude and phase of the meta-atom as functions of the width of the upper cuboid cavity w under different incident angles. (e) Scattering acoustic field distributions of the coded meta-atoms (0 to 7) at 3430 Hz.

Table 1. Selected widths w, corresponding codes, and reflection phases of the meta-atoms.

w (mm)	3	3.75	4.07	4.25
Code	0	1	2	3
Phase (deg)	28.88	73.57	119.18	165.53
w (mm)	4.44	4.68	5.29	9.88
Code	4	5	6	7
Phase (deg)	−149.66	−105.14	−60.01	−14.72

Moreover, the proposed meta-atoms are surrounded by perfectly matched layers to mimic reflectionless boundaries. The reflection amplitude and phase are obtained from the simulated reflection spectra using standard transfer matrix techniques.[42]

Figures 2(c) and 2(d) show the reflection amplitude and phase responses as functions of the width w of the upper cuboid cavity under different incidence angles of the plane wave. It is evident that the variation curves of reflection amplitude with increasing w from 0.1 mm to 10 mm under different incidence angles are largely consistent. Two local minima appear at $w = 4.3$ mm and $w = 7.2$ mm, respectively. Moreover, these amplitudes generally decrease with increasing incidence angle, except for the case of 60°. Similarly, in Fig. 2(d), although the reflection phase response varies slightly under different incidence angles, the curves almost overlap across the variation of w. Importantly, as w increases from 0.1 mm to 10 mm, a phase coverage of more than 315° is achieved at $f = 3430$ Hz. From this analysis, it can be concluded that the reflection response of the meta-atoms remains nearly unchanged when the incidence angle is below 60°. Hence, the meta-atoms exhibit insensitivity of the reflection response to the incidence angle. Furthermore, reflection phase responses of adjacent meta-atoms with a difference of approximately 45° are coded from 0 to 7, which are used to construct the CDAM. Due to the weak angular dependence of the phase response, the reflection phase curve at an incidence angle of 0° is used to select the required w. The selected w, corresponding codes, and their reflection phases are summarized in Table 1. The simulated scattering acoustic field distributions of different coded meta-atoms are further shown in Fig. 2(e), where a phase shift interval of approximately 45° can also be observed.

3. Numerical simulation of the CDAM

In the following, the far-field scattering patterns of the proposed CDAM are presented to verify its acoustic scattering reduction performance. A CDAM with bending angle α comprising $N \times N$ coding elements, each of size D, is illustrated in Fig. 3(a). The reflected phases of each coding element, $\varphi(m,n)$, take the values 0°, 45°, 90°, 135°, 180°, 225°, 270°, and 315°, respectively. Under normal incidence, the far-field scattering function of the CDAM is expressed as[43]

$$f(\theta,\varphi) = f_{\mathrm{e}}(\theta,\varphi)\sum_{m=1}^{N}\sum_{n=1}^{N}\exp\{-\mathrm{i}\{\varphi(m,n) + kD\sin\theta\,[(m-1/2)\cos\varphi + (n-1/2)\sin\varphi]\}, \quad (1)$$

where θ denotes the elevation angle, φ is the azimuth angle, and $f_{\mathrm{e}}(\theta,\varphi)$ is the far-field scattering function of the individual coding elements. Here, $k = 2\pi/\lambda$ is the wave number. The directional function $\mathrm{Dir}(\theta,\varphi)$ of the CDAM is defined as

$$\mathrm{Dir}(\theta,\varphi) = \frac{4\pi|f(\theta,\varphi)|^2}{\int_0^{\pi/2}\int_0^{2\pi}|f(\theta,\varphi)|^2\sin\theta\,\mathrm{d}\theta\,\mathrm{d}\varphi}. \quad (2)$$

According to Eqs. (1) and (2), the scattering fields of the CDAM can be controlled by adjusting its coding sequence. Therefore, it is necessary to encode the eight types of coding elements in an aperiodic sequence to enable reflected waves in multiple directions and realize diffuse reflection.

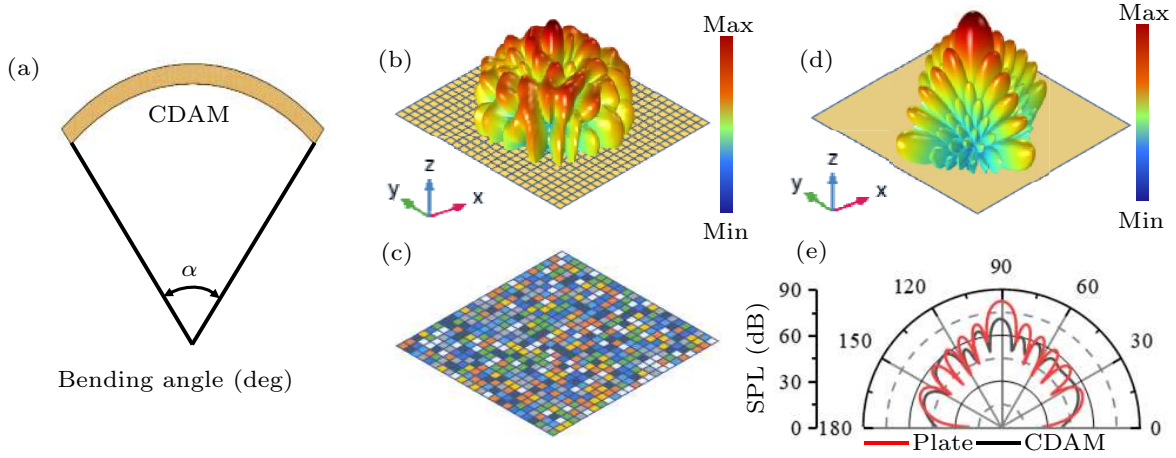


Fig. 3. (a) Schematic diagram of the CDAM with bending angle α. (b) 3D simulated scattering pattern of the CDAM at $\alpha = 0°$. (c) Quasi-random coding sequence of the proposed CDAM. (d) 3D simulated scattering pattern of a rigid planar plate with the same size as the CDAM in (b). (e) Corresponding 2D scattering patterns of the rigid plate and CDAM in the *xoz* plane.

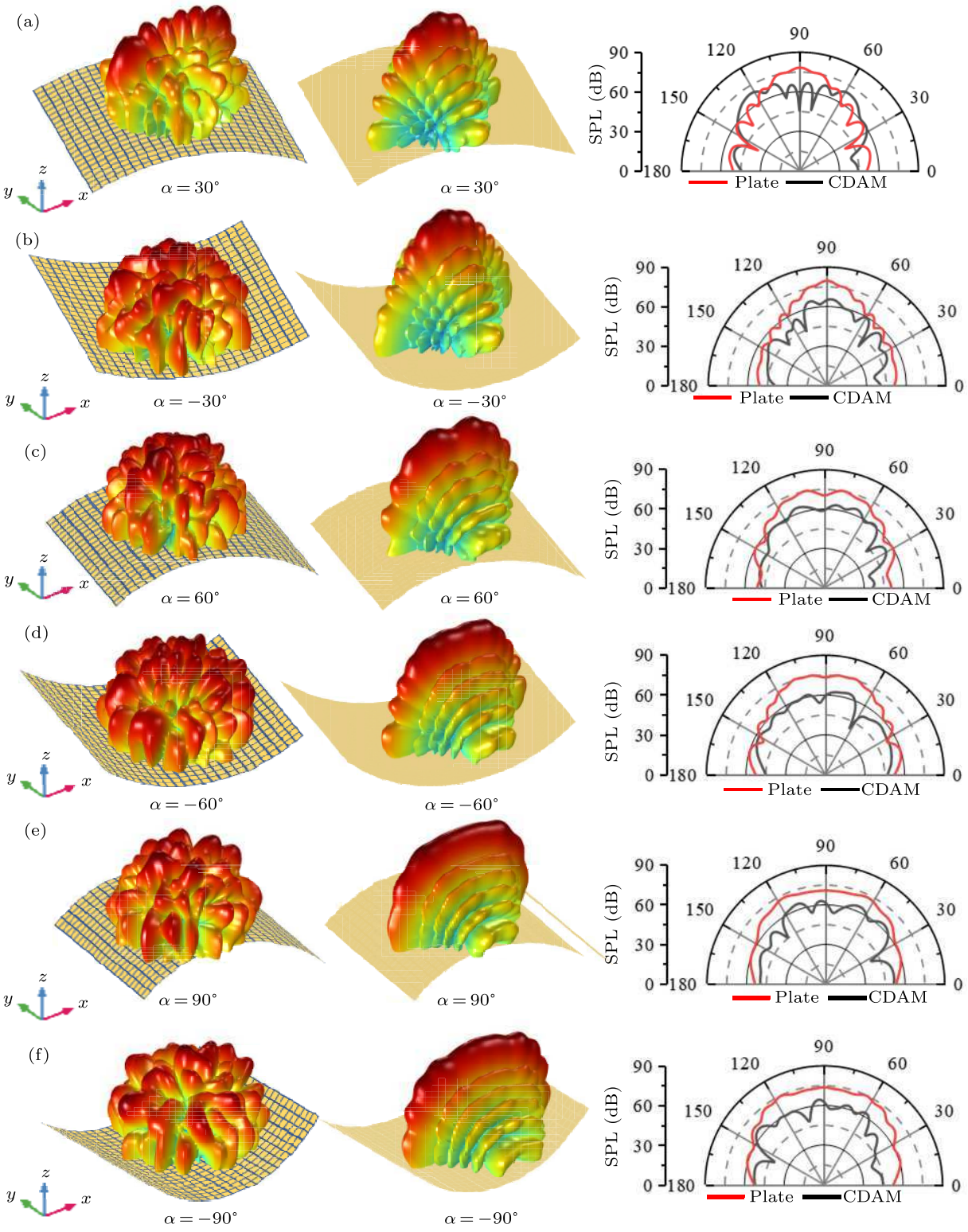


Fig. 4. Simulated scattering patterns of the CDAMs and rigid plates with the same size and shape under bending angles of ±30°, ±60°, and ±90°. The left column shows 3D scattering patterns of the CDAMs, the middle column shows 3D scattering patterns of rigid plates, and the right column shows corresponding 2D scattering patterns of both cases in the *xoz* plane.

To achieve scattering reduction via the proposed CDAM, the meta-atoms in Table 1 are used to generate a quasi-random coding sequence in MATLAB, as shown in Fig. 3(c) with color-code correspondence in Fig. 1. Under normal incidence of plane waves, when the bending angle α of the CDAM is 0°, corresponding to the planar diffusion acoustic metasurface (PDAM), the reflected wave energy is dispersed into multiple directions due to destructive interference between the meta-atoms (Fig. 3(b)). In contrast, a rigid planar plate of the same size is shown in Fig. 3(d), producing a strong specular beam. Comparison of Figs. 3(b) and 3(d) demonstrates that the proposed CDAM achieves significant scattering reduction in the

specular direction.

The corresponding 2D scattering patterns of the rigid plate and CDAM in the *xoz* plane are shown in Fig. 3(e) to quantitatively evaluate scattering reduction, where black and red curves represent the far-field sound pressure levels (SPLs) of the CDAM and plate, respectively. The scattering reduction value, $R(\alpha)$, is defined as the difference in far-field SPL between the rigid plate and the CDAM in the specular direction

$$R(\alpha) = \mathrm{SPL}_{\mathrm{Plate}}(\alpha) - \mathrm{SPL}_{\mathrm{CDAM}}(\alpha), \tag{3}$$

where $\mathrm{SPL}_{\mathrm{Plate}}$ and $\mathrm{SPL}_{\mathrm{CDAM}}$ denote the SPLs of the rigid plate and CDAM, respectively. For the case $\alpha = 0°$, the specular scattering reduction $R(0°)$ is approximately 11.64 dB, confirming that the planar CDAM provides excellent backward scattering suppression.

More importantly, to demonstrate that the proposed CDAM maintains excellent scattering reduction at different bending angles, 3D scattering patterns and the corresponding 2D patterns in the *xoz* plane for the CDAM and rigid plates of the same size and shape are shown in Fig. 4. Specifically, the coding sequences of the CDAM in Fig. 4 are the same as those in Fig. 3, and both concave (negative bending angle) and convex (positive bending angle) CDAMs are implemented with bending angles of $\pm 30°$, $\pm 60°$, and $\pm 90°$.

As shown in Fig. 4, the curved CDAM disperses incident acoustic energy in all directions, whereas the curved rigid plates reflect energy primarily around the *xoz* plane. The 2D scattering patterns in the *xoz* plane further confirm that, for the curved CDAM, scattering reductions (R) are at least 9 dB when comparing the far-field SPLs of the CDAMs and plates in the specular direction at bending angles of $\pm 30°$, $\pm 60°$, and $\pm 90°$, as shown in the right column of Fig. 4. Therefore, dispersive scattering continues to provide excellent scattering reduction for curved CDAMs. Additional results for other frequencies and the mechanical properties of the CDAM and meta-atoms are provided in the supplementary materials.

To quantitatively illustrate the influence of the bending angles on scattering reduction, Fig. 5 further compares the SPLs of the CDAM and curved plates in the specular direction under different bending angles. The results indicate that scattering reduction depends on the bending angle. For negative bending angles of $-30°$, $-60°$, and $-90°$, the scattering reductions (R) are approximately 14.93 dB, 14.8 dB, and 10.51 dB, respectively. For positive bending angles of 30°, 60°, and 90°, the scattering reductions (R) are approximately 32.69 dB, 11.62 dB, and 9.03 dB, respectively.

It is evident that for positive bending angles, the scattering reduction decreases as the bending angle increases. For a convex rigid plate, as the bending angle increases, acoustic energy in the specular direction spreads to the sides, causing a significant SPL reduction in that direction. In contrast, the SPL of the CDAM in the specular direction remains low and varies smoothly. Consequently, when the reference SPL of the rigid plate decreases significantly due to bending, the absolute difference between the SPLs of the rigid plate and the CDAM also decreases.

Nevertheless, as shown in Figs. 4 and 5, the proposed CDAM exhibits significant sound diffusion regardless of bending angle, highlighting its potential for stealth and noise control on complex curved surfaces.

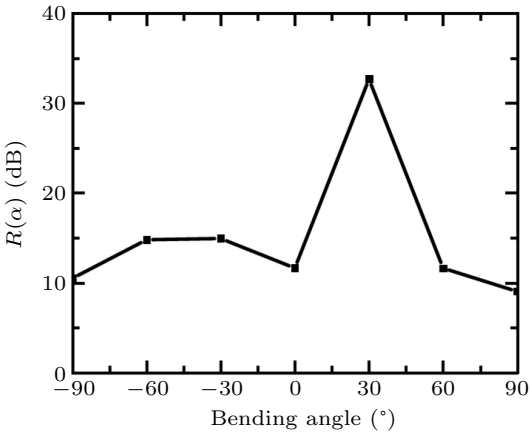


Fig. 5. Scattering reduction $R(\alpha)$ in the specular direction as a function of bending angle, obtained by comparing the far-field SPLs of the CDAM and rigid plates of the same size and shape.

Table 2. Comparison of the CDAM with representative acoustic diffusers.

Ref. No.	Material type	Structural configuration	Bending adaptability	Scattering reduction performance	Operating bandwidth
[20]	ABS (rigid)	Helmholtz-like resonator	no bending	normalized diffusion coefficient ~ 0.5	6860–11517 Hz
[23]	elastic membrane + aluminum frame (rigid)	membrane-type resonator	no bending	diffusion coefficient 0.22	1000 Hz
[24]	PLA (rigid)	flipped holey meta-atoms	no bending	none	5400–6200 Hz
[30]	photopolymer (rigid)	dual-cavity meta-atoms	no bending	> 8 dB	5800–6200 Hz
[31]	steel-based pentamode (rigid)	hexagonal meta-atoms	no bending	≈ 10 dB	7450 Hz
[32]	photopolymer (rigid)	labyrinth and Helmholtz-like resonator	no bending	> 15 dB	6550–6950 Hz
This work	PDMS (soft)	Helmholtz-like resonator	±90° bending	> 9 dB	3430 Hz

In addition, to highlight the advantages of the proposed CDAM, Table 2 provides a comparative summary between the proposed CDAM and several representative studies on sound diffusion from the literature. Owing to the use of PDMS, the proposed CDAM simultaneously exhibits two key advantages: a large bending angle and excellent scattering reduction. The relatively low Young's modulus of PDMS allows large deformations up to $\pm 90^\circ$ while maintaining structural integrity. Moreover, compared to other flexible deformable structures,[44,45] such as origami-based designs and stretchable circuits, the proposed Helmholtz-resonance-like meta-atom offers additional benefits, including flexible wavefront manipulation, a simple structure, and ease of fabrication.

4. Discussion

While numerical simulations demonstrate the promising performance of the proposed CDAM, its experimental realization presents challenges in fabricating soft CDAMs and characterizing acoustic fields on curved surfaces. To address these challenges, we outline a feasible experimental approach. For fabrication, two-photon direct laser writing using a liquid-phase PDMS-based photomaterial enables high-precision 3D printing of the complex coding elements.[46] For accurate acoustic field measurements on curved surfaces, a far-field scattering measurement scheme can be employed,[32] where the far-field SPL is recorded to quantitatively evaluate the scattering reduction of the CDAM. These established methods provide a reliable route for future experimental validation.

5. Conclusion

In summary, we have proposed a CDAM composed of soft materials capable of advanced sound diffusion and excellent backward scattering reduction. The CDAM consists of eight types of meta-atoms with a 45° phase difference. Simulation results demonstrate that the proposed CDAM achieves scattering reductions of at least 9 dB across different bending angles when comparing the far-field SPLs of the CDAM with those of curved rigid plates in the specular direction. Compared with traditional PDAMs, the use of soft materials allows the CDAM to bend freely, adapting to various curved surfaces and substantially enhancing its practical utility.

Acknowledgments

This work was supported by the National Natural Science Foundation of China (Grant Nos. 52305099, 52305249, and 12562014) and the Guizhou Provincial Basic Research Program (Natural Science) (Grant No. MS (2026) 187).

References

[1] Han C, Fan S, Zhou H T, *et al.* 2025 *Nat. Commun.* **16** 634
[2] Zhang H, Wang Q, Fink M and Ma G 2024 *Nat. Commun.* **15** 1270
[3] Surappa S, Pavagada S, Soto F, Akin D, Wei C, Degertekin F L and Demirci U 2025 *Nat. Commun.* **16** 494
[4] Dong H W, Shen C, Liu Z, *et al.* 2024 *Mater. Today (Amst.)* **80** 824
[5] Li R, Jiang Y, Zhu R, Zou Y, Shen L and Zheng B 2022 *Sci. Rep.* **12** 12037
[6] Zhu Y and Assouar B 2019 *Phys. Rev. Mater.* **3** 045201
[7] Zeng H, He Z, Wu Y, Gao S, Mao F, Fan H, Fan X, Kan W, Zhu Y, Zhang H and Assouar B 2024 *Adv. Funct. Mater.* **34** 2405132
[8] Tian Z, Meng Y, Zhao S, Wang Y and Chang Z 2025 *Mech. Syst. Signal Process.* **223** 111849
[9] Li Y, Shen C, Xie Y, Li J, Wang W, Cummer S A and Jing Y 2017 *Phys. Rev. Lett.* **119** 035501
[10] Huang S, Wen G, Yin S, Lv Z, Liu J, Pan Z and Jian L 2024 *J. Sound Vib.* **591** 118628
[11] Fan S W, Zhu Y, Cao L, Wang Y F, Chen A L, Merkel A, Wang Y S and Assouar B 2020 *Smart Mater. Struct.* **29** 105038
[12] Tang Y, Zhang Y, Xie B, Cheng H, Tian J and Chen S 2022 *Phys. Rev. Appl.* **17** 044027
[13] Qu R, Guo J, Fang Y, Zhong S and Zhang X 2023 *Mech. Syst. Signal Process.* **204** 110782
[14] Yan J, Li Y, Peng Y and Yao S 2024 *Thin-Walled Struct.* **199** 111839
[15] Quan J, Sun B, Fu Y, Gao L and Xu Y 2024 *Chin. Phys. Lett.* **41** 014301
[16] Schroeder M R 1975 *J. Acoust. Soc. Am.* **57** 149
[17] Schroeder M R 1979 *J. Acoust. Soc. Am.* **65** 958
[18] Ballestero E, Jiménez N, Groby J P, Aygun H, Dance S and Romero-García V 2021 *Appl. Phys. Lett.* **119** 044101
[19] Ballestero E, Jimenez N, Groby J P, Dance S, Aygun H and Romero-García V 2019 *Appl. Phys. Lett.* **115** 081901
[20] Zhu Y, Fan X, Liang B, Cheng J and Jing Y 2017 *Phys. Rev. X* **7** 021034
[21] Fan X D, Zhu Y F, Liang B, Yang J, Yang J and Cheng J C 2017 *Appl. Phys. Lett.* **111** 103502
[22] Jiménez N, Groby J P and Romero-García V 2021 *Sci. Rep.* **11** 10217
[23] Zhao H, Guan X, Jia H, Yang Y, Bi Y, Gai X, Li X and Yang J 2021 *Appl. Phys. Express* **14** 094005
[24] Shi J, Liu C, Guo C, Chu H, Liu X, Christensen J and Lai Y 2022 *Phys. Rev. Appl.* **18** 064064
[25] Liang T, He M, Dong H W, Xia L and Huang X 2023 *Mech. Syst. Signal Process.* **192** 110226
[26] Chen Y, Cao W H, Li J Q, *et al.* 2025 *Chin. Phys. B* **34** 044205
[27] Yang H L, Ni B, Guo J H, Zhou H and Chang J H 2025 *Chin. Phys. B* **34** 050702
[28] He S, Cao W, Nie K, Ye J, Hu J and Wu L 2025 *iScience* **28** 112402
[29] Zhao S D, Dong H W, Miao X B, Wang Y S and Zhang C 2022 *Phys. Rev. Appl.* **17** 034019
[30] Cao W K, Wu L T, Zhang C, Ke J C, Cheng Q and Cui T J 2019 *J. Appl. Phys.* **126** 194503
[31] He L, Cai L and Chen X 2021 *J. Appl. Math. Phys.* **9** 1829
[32] Xiao L, Cao W, He S, Yang J, Hu J and Chen M 2024 *Appl. Acoust.* **224** 110136
[33] Fan S W, Zhao S D, Cao L, Zhu Y, Chen A L, Wang Y F, Donda K, Wang Y S and Assouar B 2020 *Phys. Rev. B* **101** 024104
[34] Du X Y, Chen A L and Wang Y S 2025 *Mech. Syst. Signal Process.* **232** 112710
[35] Sun K, Zhang F, Chen S, Fu Q, Zeng Y and Fan Y 2024 *iScience* **27** 110504
[36] Wang H, Han Q and Lv H 2025 *Appl. Acoust.* **240** 110894
[37] Liu Y, Cao G, Liu C and Ma F 2025 *Appl. Acoust.* **228** 110314
[38] Meng Z, Wang L and Wang J 2023 *Extreme Mech. Lett.* **61** 102023
[39] Jin Y, Kumar R, Poncelet O, Mondain-Monval O and Brunet T 2019 *Nat. Commun.* **10** 143
[40] Tang H, Chen Z, Tang N, Li S, Shen Y, Peng Y, Zhu X and Zang J 2018 *Adv. Funct. Mater.* **28** 1801127
[41] Kumar R, Jin Y, Marre S, Poncelet O, Brunet T, Leng J and Mondain-Monval O 2021 *J. Porous Mater.* **28** 249
[42] Song G Y, Cheng Q, Cui T J and Jing Y 2018 *Phys. Rev. Mater.* **2** 065201
[43] Cui T J, Qi M Q, Wan X, Zhao J and Cheng Q 2014 *Light: Sci. Appl.* **3** e218
[44] Benouhiba A, Rougeot P, Andreff N, Ouisse M and Rabenorosoa K 2024 *Smart Mater. Struct.* **33** 105042
[45] Robinson A, Aziz A, Liu Q, Suo Z and Lacour S P 2014 *J. Appl. Phys.* **115** 143511
[46] Xu X, Qiu Y, Chen C Y, *et al.* 2025 *Lab Chip* **25** 1947